

Multi-Modal Fingerprint Presentation Attack Detection: Evaluation On A New Dataset

Leonidas Spinoulas*, Hengameh Mirzaalian*,
Mohamed Hussein, Member, IEEE, and Wael AbdAlmageed, Member, IEEE

Abstract—Fingerprint presentation attack detection is becoming an increasingly challenging problem due to the continuous advancement of attack preparation techniques, which generate realistic-looking fake fingerprint presentations. In this work, rather than relying on legacy fingerprint images, which are widely used in the community, we study the usefulness of multiple recently introduced sensing modalities. Our study covers front-illumination imaging using short-wave-infrared, near-infrared, and laser illumination; and back-illumination imaging using near-infrared light. Toward studying the effectiveness of each of these unconventional sensing modalities and their fusion for liveness detection, we conducted a comprehensive analysis using a fully convolutional deep neural network framework. Our evaluation compares different combination of the new sensing modalities to legacy data from one of our collections as well as the public LivDet2015 dataset, showing the superiority of the new sensing modalities in most cases. It also covers the cases of known and unknown attacks and the cases of intra-dataset and inter-dataset evaluations. Our results indicate that the power of our approach stems from the nature of the captured data rather than the employed classification framework, which justifies the extra cost for hardware-based (or hybrid) solutions. We plan to publicly release one of our dataset collections.

Index Terms—Fingerprint Biometrics, Presentation Attack Detection, Multi-Spectral Imaging, Short-Wave Infrared, Convolutional Neural Networks.

1 INTRODUCTION

BIOOMETRIC authentication systems provide additional security and convenience as well as reduced cost, compared to conventional authentication methods. As a result, their use is widespread in different application domains, including law-enforcement or border and access control, for government, corporate or personal purposes. Nevertheless, such systems can be vulnerable to different types of attacks targeting different points of the underlying authentication pipeline. Arguably, the most vulnerable component of a biometric authentication system is the biometric sensor itself, due to the public accessibility of sensors, in many cases. An attack on a biometric sensor typically constitutes the presentation of a fake sample in order to either (1) impersonate a legitimate user or (2) conceal the true identity of a black-listed one. Automatic detection of this type of *presentation attack* (PA) has attracted significant research interest with a myriad of *presentation attack detection* (PAD) methods applied on different biometric modalities, such as fingerprint, iris or face [1]. However, due to the continuous advent of realistic *presentation attack instruments* (PAIs), PAD is still an increasingly challenging problem.

Fingerprint is perhaps the first modality to be used for biometric authentication, and hence, has been thoroughly studied by the biometrics and computer vision communities [2]. Despite its wide acceptability as a universal, distinc-

tive, and permanent biometric characteristic [3], presentation attacks have been shown to successfully spoof fingerprint authentication systems [4], [5]. As a result, significant research work has been devoted to address the problem of *fingerprint presentation attack detection* (FPAD) [6], [7].

FPAD methods can be categorized into *software-only* or *hybrid*, based on the components they add to the biometric authentication system. *Software-only* or *software-based* techniques, which are the most abundant in the literature, only add a software module to augment existing fingerprint authentication systems with PAD functionality. Hence, they solely depend on the data used for enrollment and recognition to perform FPAD. Examples of *software-based* techniques include [8], [9], [10], [11], [12], [13], [14]. On the contrary, *hybrid* or *hardware-based* techniques employ additional hardware for FPAD along with the hardware used for fingerprint sensing. We refer to them as *hybrid* techniques since they still involve software modules that process the data captured by the additional sensing hardware to deliver FPAD functionality. Examples of *hybrid* techniques include [15], [16], [17].

Software-only FPAD techniques have attracted more interest in the research community owing to their cost-effectiveness and direct applicability on publicly available datasets. Nonetheless, we argue that *hybrid* techniques should gain more attention for the following reasons:

- L. Spinoulas, H. Mirzaalian, M. Hussein, and W. AbdAlmageed are with the Information Sciences Institute (University of Southern California), Marina Del Rey, CA, 90292.
M. Hussein is also with the Faculty of Engineering, Alexandria University, Alexandria, Egypt 21544.
E-mail: lspinoulas@isi.edu, hengameh@isi.edu, mohamedhussein@isi.edu, walmageed@isi.edu

The asterisk * next to author names denotes equal contribution.

- Authentication and PAD are two fundamentally different problems. Hence, restricting them to rely on the same sensing hardware limits the progress that could be attained in each.
- With the continuous evolution of sophisticated PA techniques and the attackers' deeper understanding of the intrinsics of biometric authentication, it is

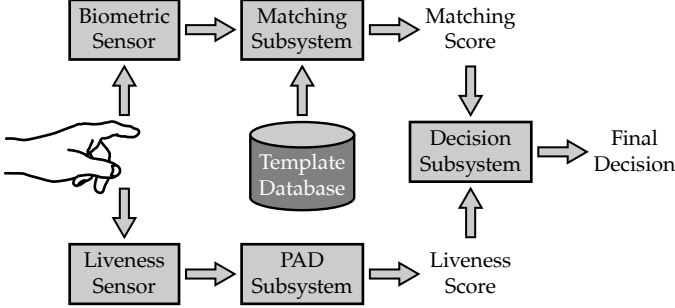


Fig. 1. A biometric authentication system with a hybrid fingerprint presentation attack detection (FPAD) subsystem.

becoming increasingly challenging to rely on a single sensing technology for both authentication and PAD. In fact, it has been shown that each of the major fingerprint sensing technologies (e.g., optical, capacitive or thermal) is vulnerable to at least one type of material used for PAIs (e.g., gelatin, silicone or glycerin) [18], [19], [20], [21].

- Not only attack fabrication technology improves but also the effect of attacks is becoming more devastating, especially when a single successful attack can be used to impersonate multiple individuals at the same time [22], [23]. Consequently, especially for security critical applications, the additional hardware cost of *hybrid* approaches is well justified.
- *Hybrid* PAD techniques can enhance the reliability of a biometric authentication system. Consider the system illustrated in Fig. 1 which employs a hybrid PAD subsystem with a parallel matching branch (similar to the one introduced in [24]). In this design, the separation between the matching and PAD pipelines enhances security since an attacker would have to simultaneously compromise both processing pipelines to succeed. Such task is more challenging compared to the single-point attacks typically found in *software-only* PAD approaches [25].

In this paper, we focus on *hybrid* techniques and evaluate a number of recently introduced sensing modalities for FPAD against legacy data from fingerprint authentication systems. Specifically, we investigate the performance of a novel fully-convolutional neural network (FCN) model for FPAD on images captured under different illumination conditions, namely:

- 1) *Visible* (VIS) and *near-infrared* (NIR), denoted together as F_M .
- 2) *Short-wave-infrared* (SWIR), denoted as F_S .
- 3) *Laser speckle contrast imaging* (LSCI), denoted as F_L .
- 4) *Near-infrared back-illumination*, denoted as B_N .

In this notation, the letter F stands for front-illumination-based sensing, in which the illumination source and the camera are on the same side with respect to the finger; and the letter B stands for back-illumination-based sensing, in which the illumination source and the camera are on two opposite sides of the finger. The two types of illumination are illustrated in Fig. 2. The subscripts in the aforementioned notation refer to the type of illumination used. To assess

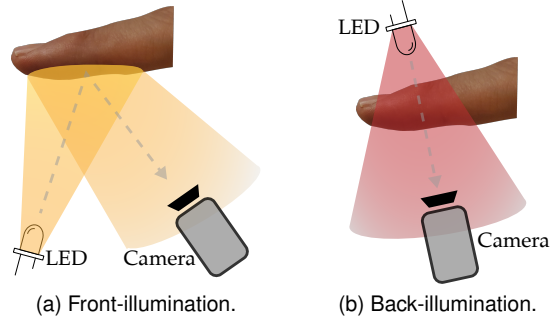


Fig. 2. Front vs. Back Illumination

the value of *hybrid* techniques, the performance of our FPAD model using these modalities – individually or in different combinations with one another – is compared to the performance of the same model on legacy fingerprint images, used in *software-only* techniques. We will refer to the unconventional sensing modalities data as *prototype data*.

The performance evaluation in this paper is conducted over a new large dataset, named Presentation Attack Detection from Information Sciences Institute (*PADISI*). *PADISI* includes data from three different biometric modalities: fingerprint, face, and iris that were collected using the developed system in [26]. In this paper, we only study the fingerprint portion, which we will refer to as *PADISI-Finger*. *PADISI* was collected at two different sites. The first site is the University Park Campus of the University of Southern California (*USC*), in Los Angeles, California while the second is in Columbia, Maryland in a facility of the Applied Physics Laboratory (*APL*) of John Hopkins University. The data at the two sites were collected using two different replicas of the system in [26]. Additionally, the *APL* collection included legacy fingerprint data collected via a number of commercial fingerprint sensors. Most of the analysis in this paper is done on the *USC* data. This dataset will become publicly available upon the acceptance of this manuscript. The *APL* collection is used for inter-site evaluation and for comparison with legacy data. The public release of the *APL* data is beyond the control of the authors in this work.

The work presented in this paper builds on top of our prior work [27], [28], with the following additional notable contributions:

- This is the first study that analyzes the PAD capabilities of unconventional sensing modalities for fingerprint compared to legacy data. Our results highlight the power of the studied sensing modalities in tackling different types of attacks.
- The SWIR and LSCI data in the new datasets have significantly higher resolution (~ 192 ppi – pixels per inch) compared to the data used in our prior work [27], [28]. The resolution in the old data was only ~ 35 for SWIR and ~ 135 for LSCI.
- Our evaluation covers each unconventional modality individually as well as their combinations and compares all that to the performance on legacy data. Such thorough analysis provides valuable information to practitioners on the complementary nature among

groups of sensing modalities and their power in comparison to legacy data.

- We employ a novel FCN model, which is more efficient and more powerful than our prior patch-based convolutional neural network (CNN) models [27], [28]. To validate the effectiveness of this model, we present its evaluation on the LivDet2015 dataset [29] achieving superior performance to state-of-the-art.
- Our evaluation protocols cover a wide spectrum of scenarios. We use 3-fold cross-validation on the USC collection to assess the power of different sensing modalities. Additionally, we follow an inter-collection evaluation (training on *USC* and testing on *APL* data) to assess the effect of changes in demographic and PAI distributions. Finally, we follow a leave-one-attack-category out cross-validation to assess the performance on completely unseen attacks.
- The data collected at *USC* will be publicly released upon the acceptance of this manuscript, which constitutes a valuable asset to the research community. To our knowledge, this will be the first public dataset covering such a broad range of sensing modalities for FPAD. The dataset is relatively large and covers a wide range of PAI species.

1.1 Related Work

Aside from *alteration detection*, in which the focus is on detecting a physical alteration to a real finger for the purpose of hiding real identity, FPAD methods typically attempt to find characteristics in the input presentation that can distinguish a live finger from a dead or fake one [7]. This explains why these methods are collectively referred to as *liveness detection* [7].

Numerous proposed approaches are based on physiological characteristics of the finger that are directly sensed as part of the biometric authentication system. These characteristics can be either static or dynamic. *Static* characteristics, such as odor [16], skin resistance [30], [31], perspiration [32], and internal finger structure measured by optical coherence tomography (OCT) [17], [33], [34], [35], are typically extracted from a single image of the fingerprint. Other methods exploit multiple images to extract static characteristics, such as techniques based on multi-spectral imaging (MSI) [36], [37], [38], [39], [40], [41], [42] or multi-view imaging [43]. On the other hand, *dynamic* characteristics are derived by nature when processing multiple fingerprint images, e.g., a time series of images to measure finger distortion and elasticity [13], [44], heartbeat [14] or blood flow [45], [46].

Most of the aforementioned approaches are *hybrid* techniques since they involve additional hardware components for detecting certain physiological characteristics. However, the distinction between bona-fides and attacks may not only rely on the lack of liveness-related physiological attributes but also on the existence of artifacts on a fake fingerprint, stemming from its fabrication process. Consequently, most *software-only* techniques attempt to differentiate between bona-fide and attack samples based on pattern recognition and signal processing techniques without making the distinction between liveness detection or artifact detection.

Traditionally, *software-only* FPAD methods apply conventional classification techniques (e.g., support vector machines - SVMs) using hand-crafted features such as wavelet and gray level co-occurrence matrix of optical images [8], [47], [48], [49], histogram and binarized statistical image features [50], [51], [52], scale-invariant feature descriptors [53], Weber local descriptor [54], frequency domain information [55], and pore location distribution [56].

More recently, many *software-only* FPAD approaches have been proposed utilizing CNNs [57], [58], [59], [60]. Nogueira et al. [58] fine-tuned AlexNet [61] and VGG [62] architectures to perform liveness detection of fingerprints. A classical CNN consisting of four 2D convolutional layers with a binary cross-entropy loss was used by Wang et al. [63]. Bhanu et al. [64] used triplet loss in their network to minimize the intra-class distances of the patches belonging to the same class while maximizing the inter-class distances. Chugh et al. [65], [66], [67] used MobileNet-v1 over the centered and aligned patches extracted around fingerprint minutiae to discriminate between fake and real fingerprints of optical images. Park et al. [68] included fire and gram modules within their network to learn the textures of bona-fide and PA samples. Kim et al. [69] employed deep belief networks and used contrastive divergence for FPAD.

There exist few CNN-based *hybrid* techniques for FPAD. For instance, recently, CNN models were used with LSCI [27], [28], [70] and SWIR [36], [42] imaging. MSI-based *hybrid* techniques are particularly relevant to our research. MSI can reveal distinguishing characteristics of real human skin compared to a multitude of materials used to create fingerprint PAs. In the simplest form of MSI, multiple images of a given target are captured while the target is actively illuminated by different wavelengths in each frame. Each wavelength exhibits varying penetration, absorption and reflection properties for different materials. These phenomena can be utilized in distinguishing real human skin from other materials. Row et al. first introduced MSI to fingerprint image acquisition in [38] but all wavelengths were in the visible spectrum; specifically 430nm-630nm and white. Response to visible spectrum illumination significantly varies between different skin tones, which limits its utility for FPAD. Very limited applications of MSI in FPAD beyond the visible domain exist, such as the work on the visible and near infrared spectrum (i.e., 400nm-850nm) [71], and on the visible to SWIR regimes (400nm-1650nm), whose dynamic characteristics were investigated as a means of distinguishing live fingers from cadavers [40]. In both [71] and [40], very few samples were used. In this paper, we present the most comprehensive study of MSI on FPAD. Not only, our study covers wavelengths in the broad range VIS-SWIR, but also includes front, back, LED-based and laser-based illumination. Furthermore, we use relatively large datasets containing a wide variety of attacks.

2 FINGER BIOMETRICS SYSTEM DESIGN

The utilized finger biometrics sensor suite has been improved and simplified compared to its previous version in [27]. In this section, we provide a brief overview of the system focusing on the rationale for using the selected sensing modalities, supported by relevant literature. The

TABLE 1
Overview of collected data per finger by the utilized finger biometric sensor suite.

Camera	VIS/NIR [72] - 1282×1026 pixels - 12 bits (stored as 16)							SWIR [73] - 320×256 pixels - 16 bits				
Sensing Modality	F_M							B_N	F_S			
Illumination	white	465nm	591nm	720nm	780nm	870nm	940nm	940nm	1200nm	1300nm	1450nm	1550nm
Illuminated Frames	1	1	1	1	1	1	1	20	1	1	1	1
Non-Illuminated Frames	1	1	1	1	1	1	1	—	4	4	4	4
												—

interested reader can refer to [26] for more technical details about the design, selected hardware components and its operation. The schematic diagram of the system is shown in Fig. 3. A finger is placed on the slit and is illuminated from the bottom side (front-illumination) by multi-spectral LEDs and a laser as well as the top side (back-illumination) by NIR LEDs while being observed by two cameras from a distance of $\sim 35\text{cm}$. Each camera is sensitive to the VIS/NIR or the SWIR spectrum, respectively. The sensor is touch-less in the sense that no platen covers the finger slit.

Each chosen sensing modality in our station provides indicative information for either the liveness of a presentation or the presence of a fabrication artifact, as follows:

- Front VIS/NIR illumination (F_M) data: NIR multi-spectral images can provide ample information about the spectral and textural characteristics of the material of a presentation [71]. Further, they can be used as legacy compatible data, as shown in [26].
- Front SWIR illumination (F_S) data: Human skin has a distinctive response in the SWIR spectrum that is independent of skin tone. In a recent study, conducted by the National Institute of Standards and Technology (NIST), the variability of skin response due to differences among people was found to be less significant than the variability due to instrument characteristics only beyond the 1100nm wavelength [75]. The same observation was confirmed in a successful application of PAD using MSI in the SWIR domain, for face biometrics [76], and more recently, using the previous version of our data, on fingerprint biometrics [27], [36], [42], [77], [78].
- Front LSCI (F_L) data: When laser light illuminates a surface, a random interference pattern, known as the speckle pattern, is formed. The pattern is affected by the roughness and/or temperature of the surface and appears static for stationary objects. However, the pattern changes over time when there is motion on the illuminated object, such as the movement of blood cells under the skin surface. In fact, blood perfusion in a tissue can be visualized [79] using LSCI by collecting a sequence of images. Therefore, LSCI measurements can constitute a useful liveness signal for FPAD. LSCI has attracted very little attention in the FPAD literature despite its interesting properties. Chatterjee et al. [80] conducted a study on the hardware and physics of LSCI and showed that there is significant difference between the biospeckle patterns of bona-fide and fake fingers. However, the study involved a very small dataset and did not actually evaluate FPAD performance. Using data from

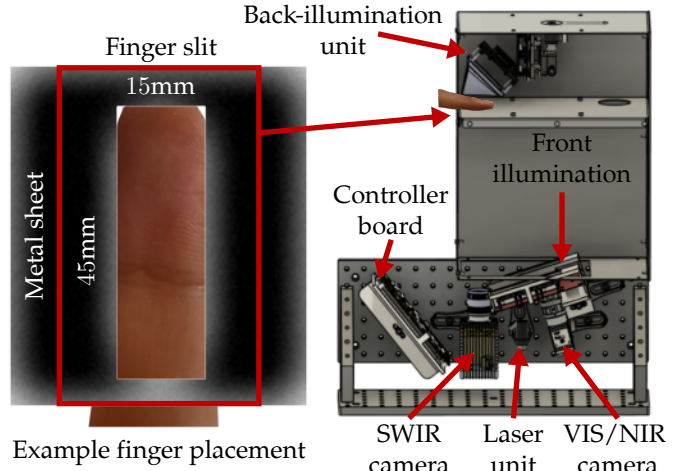


Fig. 3. Finger biometric sensor suite. See [26] for more technical details.

- the previous version of our system [27], Keilbach et al. [50], [70] performed LSCI-based FPAD by applying classical classification algorithms (e.g., SVMs), on a set of hand crafted features, such as intensity histograms or LBP features. Later on, Hussein et al. [27] and Mirzaalian et al. [28] utilized various spatio-temporal neural networks to perform LSCI-based FPAD which demonstrated promising performance.
- Back NIR illumination (B_N) data: The internal vascular pattern of a hand can be visualized using NIR illumination [71], [81]. In the presence of a finger between a light source and a camera, the collected image intensities represent the amount of light penetrating through the sample, as compared to front-illumination which measures the reflected light, instead [81]. Vessel structures appear darker since light is absorbed by the hemoglobin in the blood and can be used as an indicator of liveness for FPAD. Back-illuminated NIR images from our previous dataset were used for FPAD in [82].

It is worth noting that select combinations of the sensing modalities were already studied on the previous version of our dataset, as in [27], [53], [78], [83]. In this study, we evaluate FPAD performance on our new dataset using a comprehensive list of experiments.

A summary of the captured data for a single finger is presented in Table 1. In multiple cases, data is also captured without active illumination and such images can be used as reference frames for ambient illumination conditions. We developed two replicas of our sensor suite each one used at each collection site (USC and APL). Note that, despite

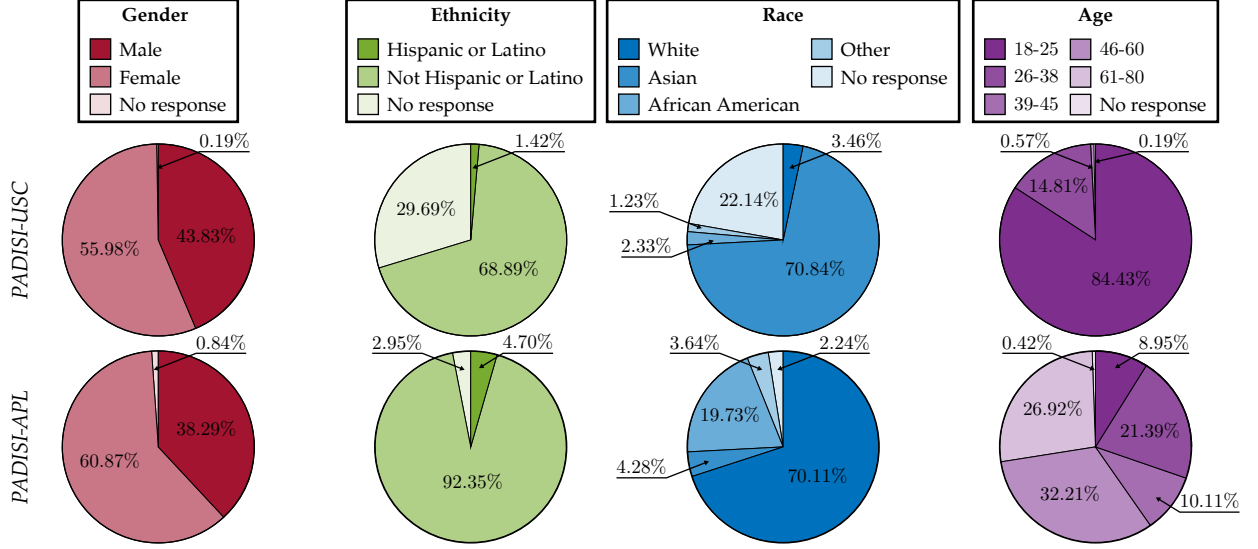


Fig. 4. Demographic information for the collected datasets. A summary of the collected samples per dataset can be found in Table 3.

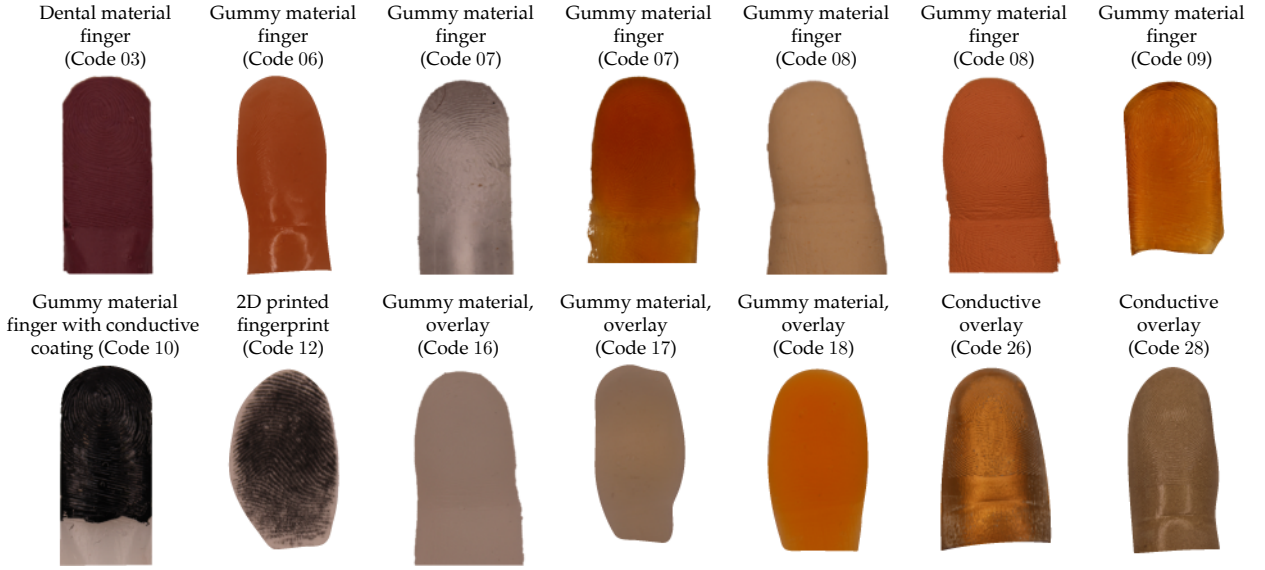


Fig. 5. Images of select PAIs used in the *PADISI-USC* data collection. More details for each PAI can be found in Table 2.

best efforts, some system adjustments could not be identical in the two replicas, such as lens shutter adjustments. Also, despite the closed-box design, ambient light might leak into the station and partially influence imaging conditions.

3 DATASET

As discussed in Section 1, the *PADISI* dataset was collected at two different sites (*USC* and *APL*). The data at *USC* were collected in two separate sessions, referred to as *USC-1* and *USC-2*, between which minor adjustments were applied on the system. During all collections, a participant presented 4 fingers from each hand (excluding little fingers). Each participant passed once or twice by the collection station either in the absence of any attack or in the presence of up to three attached PAIs to the fingers of one or both hands, while a few participants participated in multiple collection sessions. At the *APL* data collection, data was also collected

from all participants using a series of commercial legacy sensors (see [26] for details). In this work, for comparison purposes, we chose to use data from the Optical-C sensor, since it has the highest resolution and provided the most reliable data in terms of match rates (see [26]).

The collected data was thoroughly reviewed by the research team and samples with defects, e.g., due to finger motion or hardware failure, were excluded. A summary of the collected data counts, after these revisions, is provided in Table 3 while the relevant demographic information is presented in Fig. 4. As observed, the *APL* dataset is larger but exhibits a big imbalance between bona-fide and PAI samples. At the same time, the *USC* dataset contains a much larger variety of PAI species. Moreover, there is a huge discrepancy in demographics especially in terms of age and race. The *USC* dataset contains mostly young people of Asian origin (since it was collected in a university environment) while the *APL* dataset exhibits a skewed distribution

TABLE 2

PAI counts in the collected datasets. For each PAI code, we provide a general PAI description, the number of different species per dataset as well as the attributes used for grouping PAI codes in terms of material, species, transparency, and attack type. PAI categories whose appearance depends heavily on the participant and preparation method are marked with *. A summary of the collected samples per dataset can be found in Table 3. Sponsor approval is required to release additional information about each PAI code.

Description	Code	Total Samples USC	Total Samples APL	Total Species USC	Total Species APL	Grouping Attributes
Play-doh finger	01	116	—	4	—	
Silly putty finger	02	55	—	3	—	
Dental material finger	03	51	—	1	—	
Wax finger	04	74	—	1	—	
Gummy material finger	05	180	—	5	—	
	06	76	50	1	1	
	07	78	—	2	—	
	08	550	—	6	—	
	09	59	—	2	—	
	10	195	—	5	—	
Gummy material finger with conductive coating	11	69	—	1	—	
2D printed fingerprint	12	49	—	1	—	
	13	64	—	1	—	
	14	22	—	1	—	
	15	37	—	1	—	
	16	265	282	7	2	
	17	18	—	1	—	
Gummy material overlay	18	164	—	3	—	
	19	90	—	1	—	
	20	77	—	3	—	
	21*	61	314	1	4	
	22*	21	86	1	1	
	23	—	77	—	1	
3D printed finger	24	48	—	2	—	
	25	24	—	1	—	
Conductive overlay	26	72	—	1	—	
	27	—	172	—	1	
	28	98	100	1	1	
Staples/Band-aid	29	2	4	1	1	

Material

Species

Transparency

Type

Special case

TABLE 3

Collected datasets summary. Demographic information can be found in Fig. 4 while more details about PAIs are provided in Table 2.

	USC	PADISI Datasets	
	USC	APL	APL-LEGACY
Participants	355	672	665
Unique fingers	2490	5371	5308
Total samples	6211	11444	8850
Bona-fide samples	3596	10359	8043
PAI Samples	2615	1085	807
PAI Species	58	12	12

toward white people while having a more balanced age distribution. The discrepancy in the number of participants and total samples between the *APL* and *APL-LEGACY* data

in Table 3 is due to the fact that participants did not always visit the legacy sensors multiple times due to their slow speed as well as the data revision process, which was independently performed per sensor. In this table, we present only the samples from the legacy sensor that correspond to participants and fingers available in our prototype data.

Snapshots of prepared and collected PAIs are illustrated in Fig. 5. Analytic information about all PAIs used during the data collections are provided in Table 2 where PAIs are categorized using different codes, each of which can contain one or more species (e.g., referring to a different color of a specific material or a slightly different preparation method). For each PAI code, we have provided a classification scheme using a set of grouping attributes based on their material, species, transparency, and attack type. Some of these at-

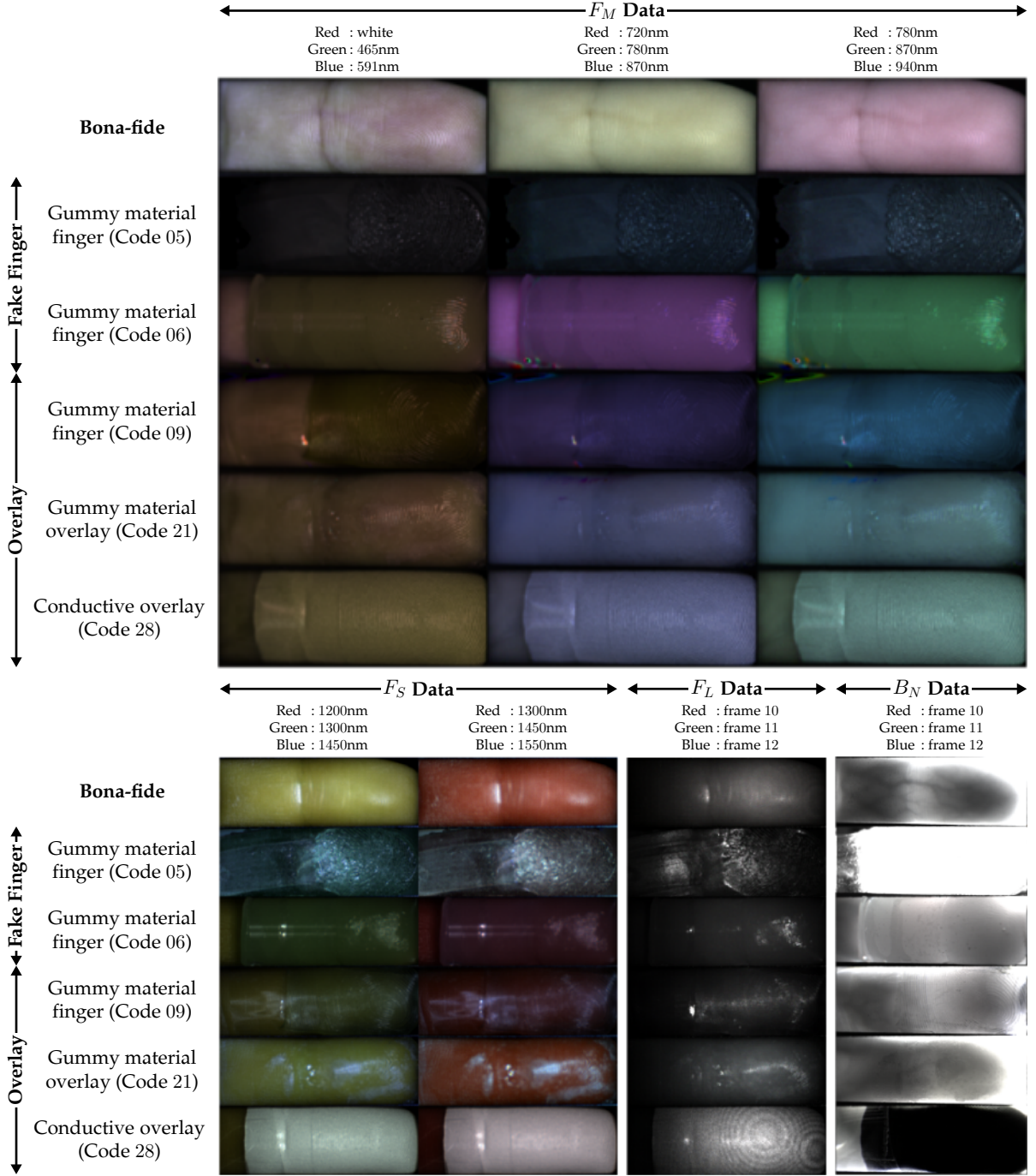


Fig. 6. RGB visualization of samples from the collected datasets for all types of captured data. For each image, the corresponding dark channel has been subtracted and each RGB channel has been normalized by dividing by its maximum value for visualization purposes, albeit introducing visible color artifacts in some cases. Note that, the resolution of the B_N data is the same as the F_M data but is presented smaller in the illustration.

tributes (e.g., transparency) were selected subjectively based on the appearance of each PAI and this classification will become important in understanding upcoming results in this work. Finally, examples of the finger area of the captured data for a bona-fide sample and select types of PAIs for all sensing modalities, described in Section 2, are provided in Fig. 6. In this illustration 3 frames are each time stacked together to form a false-colored RGB image.

3.1 Mean Intensity Analysis

Based on the appearance of the images in Fig. 6, one might argue that the average intensities of each spectral channel of the captured data could be sufficient for obtaining a reasonable FPAD performance, since the images of bona-fides and PAIs look drastically different. In order to understand the characteristics of the captured multi-spectral data in more detail, we conduct an analysis of the average intensity of each channel using t-SNE visualizations [84], where we use all available F_M and F_S data, 10 frames from

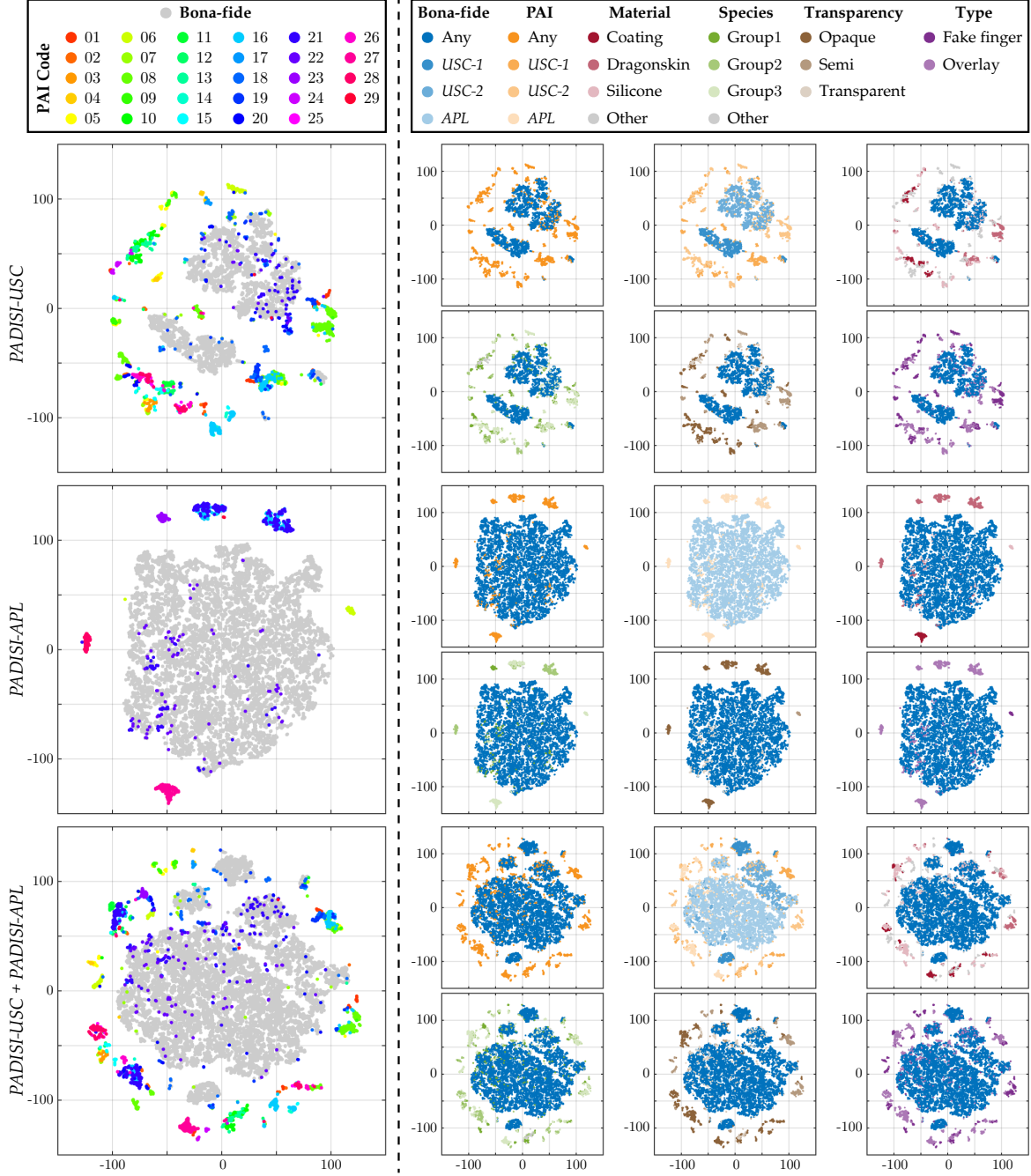


Fig. 7. t-SNE [84] visualization of average intensities of F_M , F_S , 10 frames of F_L and 3 frames of B_N data for all samples in the *PADISI* datasets. Visualizations are re-colored to distinguish data from different collections as well as bona-fides from PAIs with different characteristics.

the F_L data and 3 frames from the B_N data (see Table 1). The visualizations are presented in Fig. 7 where samples are re-colored to distinguish bona-fides from specific PAI codes, bona-fides and PAIs in general, bona-fides and PAIs from each data collection session as well as bona-fides and PAIs with the grouping attributes introduced in Table 2. From the presented 2D distributions, we can make the following observations:

- PAI codes tend to form individual clusters, supporting the use of multi-spectral data for observing the distinctive response of different PAI materials.
- Bona-fide samples of the *USC-1* and *USC-2* data

collections appear to have a large separation mainly due to the adjustments in our system (as discussed earlier). At the same time, bona-fide samples between the *USC* and *APL* data collections also exhibit significant separation possibly because of their vastly different demographics (as shown in Fig. 4).

- It is apparent that a large number of PAIs becomes separable from bona-fides simply using the average intensity features, strengthening the power of multi-spectral data for FPAD. However, the analysis demonstrates that certain PAI types might be particularly hard to detect, the majority of which are transparent overlays made of multiple materials.

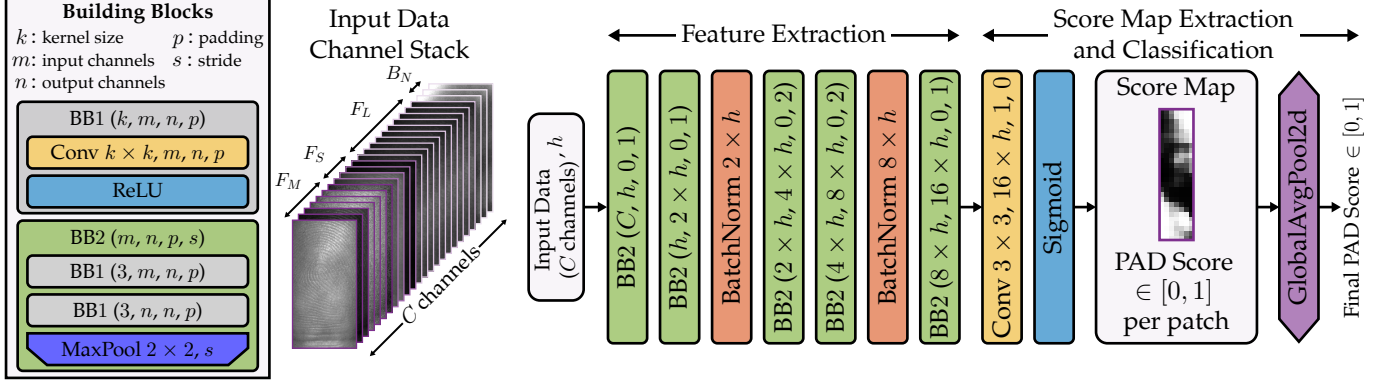


Fig. 8. Proposed FCN network architecture: Given parameter h , an input image of C channels is first converted into a two dimensional score map (corresponding to a PAD score per patch) from which the final PAD score is extracted by global average pooling.

The presented visualization can also provide an estimate of how challenging a dataset is and could be used for assigning weights to PAI codes, based on their distance from the bona-fide cluster.

4 FULLY-CONVOLUTIONAL NEURAL NETWORK MODEL

Deep neural networks (DNNs) have repeatedly delivered breakthroughs in multiple research disciplines. However, they are notoriously known for being data-hungry: substantial amounts of data have to be used to avoid overfitting during training. Despite the relatively large size of our dataset, it is still small for effectively training a DNN model. This problem has been addressed in prior work on our data in two different ways. In [27], [28], patch-based models were employed by extracting hundreds of 8×8 patches from an input sample and classifying it by taking the average score over all patches. This approach proved very effective but has two main drawbacks. First, it involves repeated computations when processing consecutive patches, which typically overlap. Second, it does not scale well as the input image size increases, in which case sparse sampling of patches becomes necessary for the approach to be feasible. The alternative approach of transfer learning was used in [42], [53], [78], where a pre-trained network is fine-tuned on our data instead of trained from scratch. The main issue with transfer learning is relying on existing models, which might be too complex for the task at hand.

In this paper, we introduce a novel model for FPAD that avoids the drawbacks of both the patch-based and transfer learning-based approaches. Our new model uses an FCN structure that maps a whole region of interest (ROI) of the input finger image to a map of classification scores, which is then averaged to produce the overall classification score of the input sample. The details of the network structure are shown in Fig. 8. The network consists of five convolutional blocks, with a batch-normalization layer after each group of two-blocks. Starting from a specified number of convolutional maps in the first block (h in Fig. 8), the number of convolutional maps is doubled in the transition between each two consecutive blocks. The final block is followed by a convolutional layer that produces a single map using a

sigmoid activation, which represents the patch-wise classification score. Note that, there are no explicitly cropped patches in the FCN model. The *patch* is an implicit concept referring to the *receptive field* of each score map element. The score map is then fed to a global average pooling (GAP) layer to produce the final score. Each score map entry is in the range $[0, 1]$, enforced by the sigmoid activation. Hence, the final model output also falls in $[0, 1]$.

The resulting PAD score can be interpreted as the probability of the presence of a PA. Hence, the ground truth score is set to 1 for PA samples and 0 for bona-fide samples. The loss function comprises of two components, one for the final classification score L_{GAP} , and one for the patch classification score L_{patch} , as:

$$L = L_{GAP} + \lambda L_{patch} , \quad (1)$$

where $\lambda > 0$. Let the score map associated with an input image x be $M : R^{C \times W \times H} \rightarrow R^{W_m \times H_m}$, where C is the number of channels in x , $W \times H$ is the input 2D image size, and $W_m \times H_m$ is the score map size. Considering the binary cross entropy (BCE) as the loss function, the two loss components can be expressed as:

$$L_{GAP}(x) = BCE \left(\frac{1}{W_m H_m} \sum_i^{W_m} \sum_j^{H_m} M_{ij}(x), t \right) , \quad (2)$$

$$L_{patch}(x) = \frac{1}{W_m H_m} \sum_i^{W_m} \sum_j^{H_m} BCE(M_{ij}(x), t) , \quad (3)$$

where $t \in \{0, 1\}$ is the ground truth label of the input x .

For all experiments presented in this work, we use $h = 16$ and $\lambda = 10$, while C is varying depending on the provided input image channels. Based on these parameters, the effective patch size (or receptive field) of the model is an area of 54×54 pixels for each score in M . Training is performed for a maximum of 100 epochs using a batch size of 16 and the Adam optimizer [85]. The initial learning rate is set to 2×10^{-4} with a minimum learning rate of 1×10^{-7} following a reduce-on-plateau by 0.5 strategy (with patience 10 epochs and threshold 1×10^{-4}) by monitoring the validation loss, when a validation set is available.

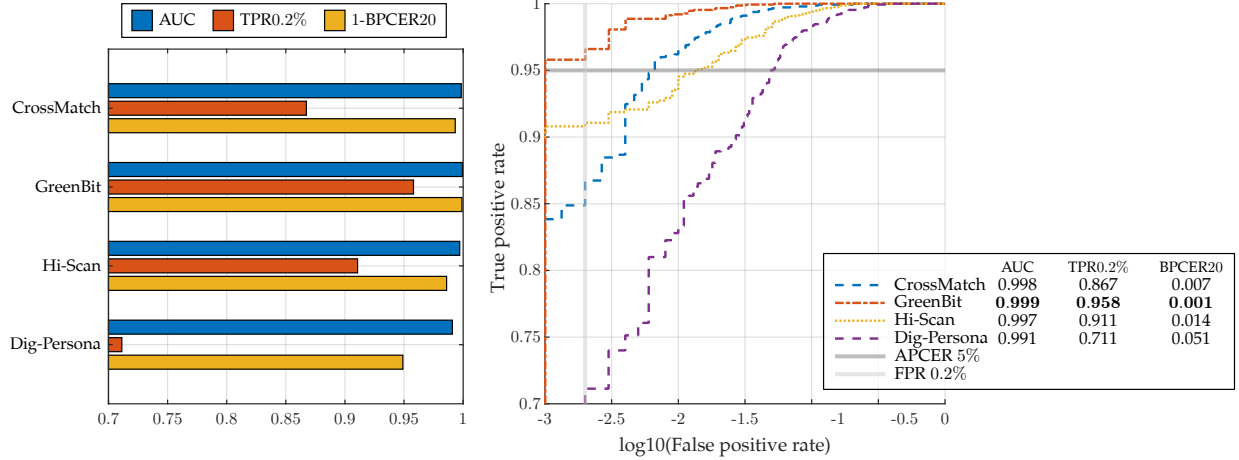


Fig. 9. FPAD evaluation on the sensors of the LivDet2015 dataset [29]. Left: Bar-graph visualization of the evaluation metrics; Right: ROC curves and analytic values (with best values highlighted in bold). The corresponding accuracies per sensor are presented in Table 4.

5 EXPERIMENTAL EVALUATION

This section presents the experimental evaluation of this work. We first study the capabilities of the presented FCN model on an existing dataset and then run a comprehensive list of experiments on the presented dataset. The analysis uses various evaluation protocols on different combinations of input channels from the collected sensing modalities in our dataset and compares their performance with legacy data, whenever appropriate. Before proceeding with the evaluation, we summarize the data pre-processing steps and evaluation metrics used in our analysis.

Data Pre-Processing: The data, whether prototype or legacy, are first pre-processed:

- **Prototype Data:** From the captured data, summarized in Table 1, we use all frames from the F_M and F_S sensing modalities, frames 10 – 19 from the F_L data and frames 10 – 12 from the B_N data, in different combinations. If non-illuminated frames are available for any spectral channel, the time-averaged non-illuminated frame is first subtracted. The data is then normalized in $[0, 1]$ using the corresponding bit depth (see Table 1). Because of the fixed relative location of the finger slit in images captured by our equipment, it was possible to set fixed ROIs for each sensing modality. The ROI was chosen to cover most of the area of the top finger knuckle which almost always consists of skin in bona-fide samples, and PAI material in PA samples. ROIs of images of different sensing modalities are all resized to 160×80 pixels using bicubic interpolation and then stacked to form the multi-spectral data cube provided to our model.
- **Legacy Data:** Legacy finger images consist of a single grayscale image where the finger ridges appear dark. We detect the finger area by first binarizing the image using thresholding, applying dilation with a circular structuring element of diameter 7 pixels and finding the centroid of the largest connected component in the resulting binary image. The centroid is used as the center for extracting an ROI of pre-defined fixed size, for all images, depending on the average finger coverage in the images of each legacy sensor.

TABLE 4
FPAD accuracy on the test sets of the LivDet2015 dataset using a threshold of 0.5. Values of existing algorithms are taken from [29] while the best performing algorithm is highlighted in bold.

Method	GreenBit	Hi-Scan	Persona	CrossMatch	Overall
nogueira	95.40	94.36	93.72	98.10	95.51
unina	95.80	95.20	85.44	96.00	93.23
jinglian	94.44	94.08	88.16	94.34	92.82
anonym	92.24	92.92	87.56	96.57	92.51
titanz	91.76	92.36	89.04	91.62	91.21
hbirkholz	91.36	93.40	88.00	89.93	90.64
hector	90.00	88.20	84.20	86.94	87.32
CSI_MM	86.56	87.84	75.56	89.99	85.20
CSI	82.12	83.20	76.20	88.33	82.71
COPILHA	72.76	75.64	79.96	69.00	74.11
UFPE II	87.68	71.24	75.44	61.16	73.33
UFPE I	82.56	64.32	78.36	59.97	70.82
Proposed	98.56	96.80	94.80	98.10	97.11

Evaluation Metrics: As discussed in Section 4, the output score of the FCN model in Fig. 8 represents the PA probability (in $[0, 1]$) of an input sample. Therefore, using a threshold of 0.5 is a natural choice for obtaining the FPAD binary classification and, hence computing the accuracy. However, any choice of threshold without a specific target operating point is indeed arbitrary. Hence, we opt to use metrics that do not depend on a pre-set threshold. In particular, three metrics are used to compare different models in our experiments: i) area under the receiver operating characteristic (ROC) curve, denoted as AUC; ii) true positive rate at 0.2% false positive rate, denoted as TPR0.2%, which is the primary evaluation metric used in IARPA’s Odin program [86], through which this research has been sponsored; and iii) bona-fide presentation classification error rate (BPCER) at attack presentation classification error (APCER) of 5%, denoted as BPCER20 in the ISO standard [87].

5.1 Evaluation on LivDet dataset

We first evaluate the proposed FCN model on the LivDet2015 dataset [29]. The dataset contains images from 4 legacy sensors, namely, CrossMatch, GreenBit, Hi-Scan and Digital-Persona from which, following the pre-processing steps for legacy data, we extracted ROIs of size 320×256 ,

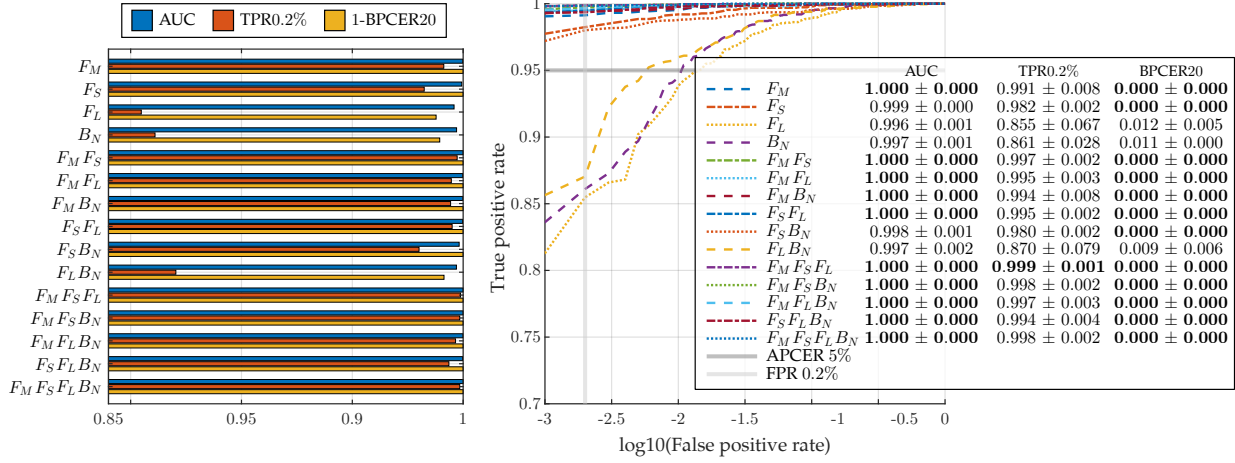


Fig. 10. 3FOLD FPAD evaluation on the *PADISI-USC* dataset. Left: Bar-graph visualization of the evaluation metrics (mean for all folds); Right: ROC curves and analytic values (mean and standard deviation for all folds with best values highlighted in bold).

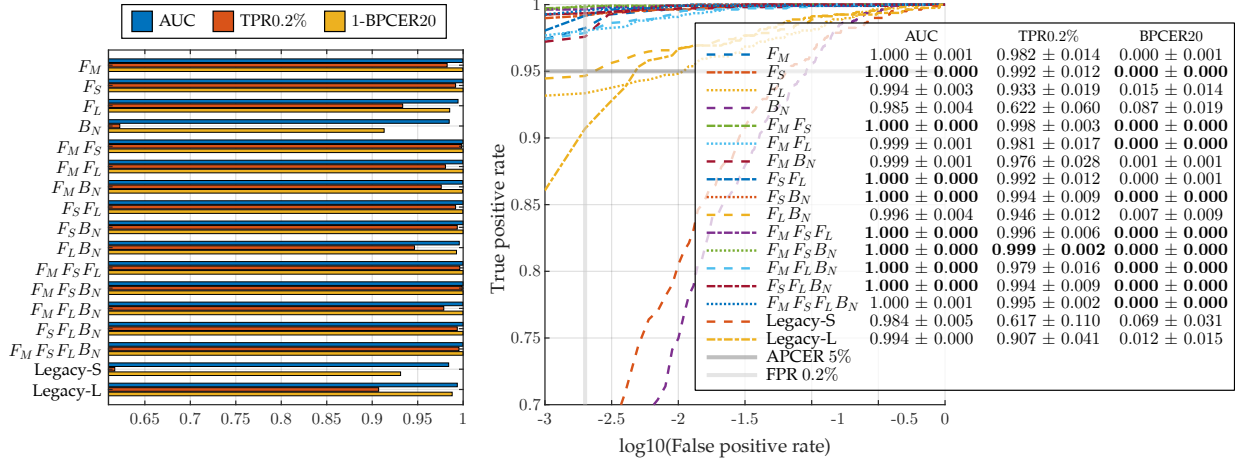


Fig. 11. 3FOLD FPAD evaluation on the *PADISI-APL* dataset and comparison with performance on legacy data (*APL-LEGACY* from Table 3). Left: Bar-graph visualization of the evaluation metrics (mean for all folds); Right: ROC curves and analytic values (mean and standard deviation for all folds with best values highlighted in bold). Legacy-S refers to “small” legacy images, equal in size to the used prototype data passed to the network, while Legacy-L refers to “large” legacy images, extracted as described in the legacy data pre-processing steps of Section 5.

320×256 , 600×480 and 260×200 pixels on the detected finger area, respectively. Images were also normalized in $[0, 1]$, based on the bit depth of 8 bits for all sensors. The LivDet2015 dataset provides pre-defined training and testing sets for each sensor but no validation set. Therefore, training was performed for the maximum of 100 epochs using the training parameters described in Section 4. The resulting ROC curves and evaluation metrics are depicted in Fig. 9 while accuracy comparison with other algorithms using a threshold of 0.5 is summarized in Table 4. As observed, the proposed model achieves state-of-the-art performance for all experiments, supporting its power for FPAD.

5.2 Evaluation on *PADISI* dataset

We now evaluate the performance of the FCN model on the *PADISI* dataset. Our analysis uses the pre-processed data cubes and, following an early-fusion approach, considers different stacked combinations of F_M , F_S , F_L and B_N data as input channels to our model under a range of evaluation protocols. Hence for each experiment in each evaluation

protocol, we vary the number of channels C , as presented in Fig. 8, to consider all possible 15 combinations of the captured sensing modalities as input data to our model.

5.2.1 Evaluation Protocols

We employ three different evaluation protocols. In the first strategy, we use a 3-fold (3FOLD) partitioning to alleviate the bias resulting from a fixed division of the dataset into training, testing, and validation sets. In this strategy, samples of a collection are divided into three roughly-equal sets of samples such that data of each participant only appears in a single set. Then, 3FOLD cross-validation evaluation is done by performing three experiments, each time using two sets for training and validation, and the left-out set for testing. Each time, from the training/validation group, 80% of data is used for training and 20% for validation, while making sure all training/testing/validation sets are participant-disjoint. It is also important to note that in all splits, the distribution of bona-fide and different PAI category samples are approximately balanced among the training/testing/validation sets. The 3FOLD partitioning is con-

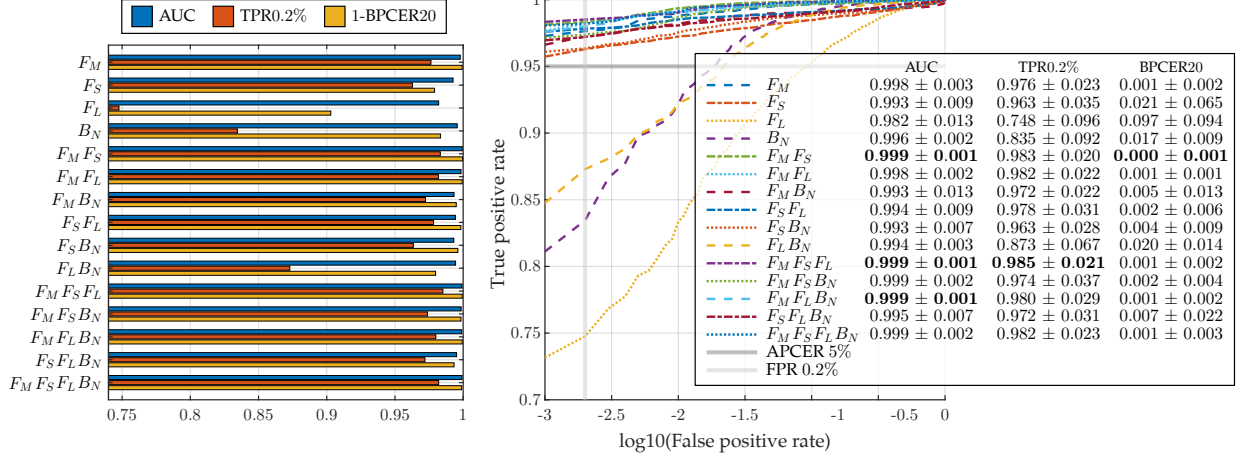


Fig. 12. LOO FPAD evaluation on the *PADISI-USC* dataset. Left: Bar-graph visualization of the evaluation metrics (mean for all LOO categories); Right: ROC curves and analytic values (mean and standard deviation for all LOO categories with best values highlighted in bold). See Table 5 for analytic results.

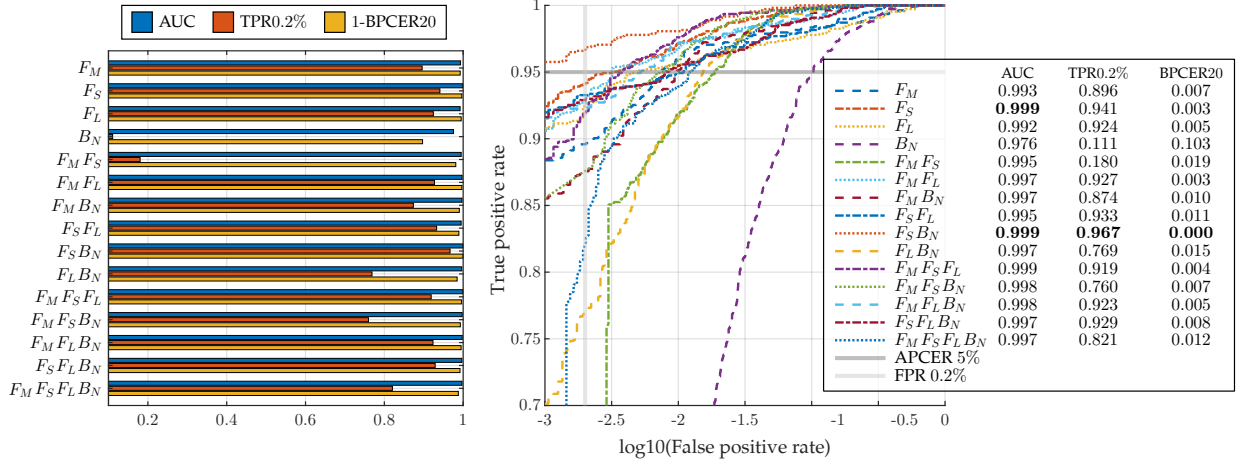


Fig. 13. Inter-site FPAD evaluation on the *PADISI* dataset (training on *USC* data and testing on *APL* data). Left: Bar-graph visualization of the evaluation metrics; Right: ROC curves and analytic values (with best values highlighted in bold).

sidered for intra-collection evaluations, which are applied either to the *PADISI-USC* or the *PADISI-APL* collections.

As a second partitioning strategy, we use a leave-one-out (LOO) protocol, in order to evaluate the ability to detect *unknown attacks* (i.e., attacks not present in the training data). Using the PAI grouping attributes of Table 2, we create a partition for each color (excluding the special case), leading to 11 partitions for the *PADISI-USC* collection.

As mentioned in Sections 2 and 3, the sensor parameters, environmental settings as well as the demographics for *PADISI* were not identical in the two collection sites (*USC* and *APL*). To study the effect of these variations to the FPAD classification performance, we also perform inter-site evaluation for which *PADISI-USC* is used for training and validation, and *PADISI-APL* is used for testing.

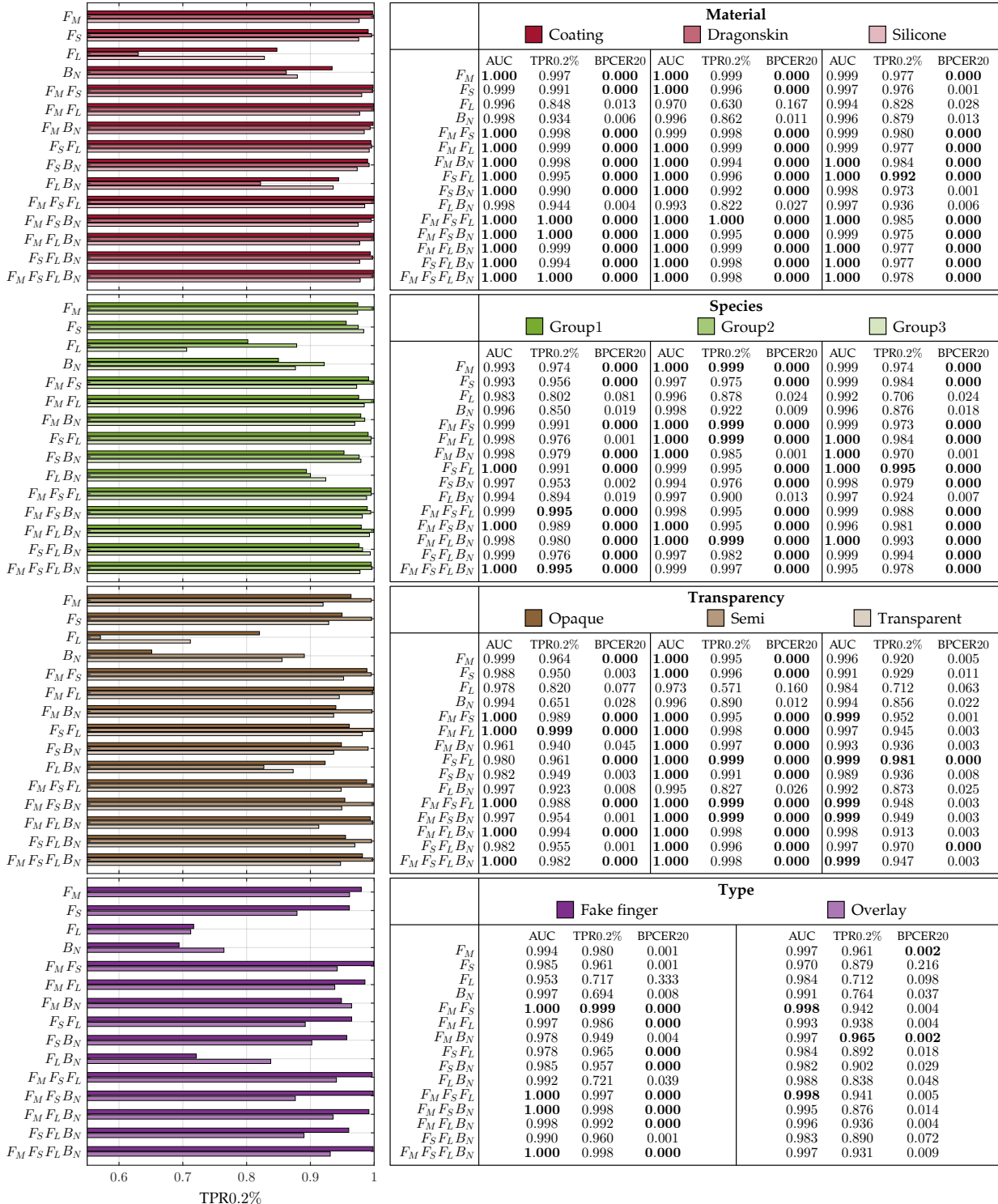
FPAD classification performance is evaluated, per fold, for each of the settings and for all aforementioned metrics. The mean and standard deviation of each metric is computed over the total number of the folds for each partitioning strategy. In the following sections, we provide an analysis of our results under the different scenarios.

5.2.2 Evaluation Results

- **3FOLD evaluation:** The 3FOLD evaluation results for the *PADISI-USC* dataset are presented in Fig. 10 and for the *PADISI-APL* in Fig. 11. For the *PADISI-APL* dataset, a comparison to the performance using the data of the selected legacy sensor is presented using two different pre-processing methods. Legacy-S refers to ROIs of 160×80 pixels, equal in size to our prototype data, while Legacy-L refers to larger ROIs of size 480×384 following the general pre-processing steps for legacy data described earlier. Even though the total number of samples for the *APL-LEGACY* data is not equal to our prototype data; the folds were consistent by using the same participant’s samples as in the 3FOLD partitions described in Section 5.2.1.
- ***PADISI-USC* LOO evaluation:** The average performance on all 11 LOO partitions of the *PADISI-USC* dataset is presented in Fig. 12 while analytic results for each partition are summarized in Table 5.
- **Inter-site evaluation:** The inter-site evaluation results are depicted in Fig. 13.

TABLE 5

Analytic LOO FPAD evaluation, per LOO category, on the *PADISI-USC* dataset. Left: Bar-graph visualization of the TPR0.2% metric; Right: Analytic values (with best values highlighted in bold). The corresponding average LOO results are presented in Fig. 12.



5.2.3 Discussion

Based on the results of Section 5.2.2 we can make the following observations:

- Some of the studied sensing modalities (particularly *F_M* and *F_S*) can achieve very high FPAD performance with *F_S* being less affected by cross-dataset

variations (as seen in Fig. 11), which is consistent with the relevant literature on SWIR imaging.

- With the exception of *F_L* or *B_N* data alone, any other single sensing modality or combination proves superior to legacy data (see Fig. 11), especially at very low false positive rates.
- In the majority of the cases, combining more than

one sensing modalities leads to improved performance. This is particularly apparent in the *unknown attack* scenario where most models employing two or more sensing modalities consistently outperform the single ones for most metrics (see Table 5). This observation supports the use of multi-spectral data for FPAD and the power of *hybrid* methods.

- In multiple cases, increasing the number of channels provided to the model does not always lead to performance improvement, albeit not with significant loss. Such behavior may signify overfitting or non-optimal weighting of certain channels toward the final classification output and could open new research directions for incorporating channel attention techniques to our model [88], [89], [90].

Extending the t-SNE visualization analysis of Section 3, we compare the separation in t-SNE space between the features extracted by the FCN model (score maps) to the corresponding mean-intensity features, for select experiments, in Fig. 14. The illustrations include results for 1 fold of the 3FOLD evaluation protocol on the *PADISI-USC* collection and the inter-site evaluation protocol. The figure presents the two worst results on the left, the medial result in the middle and the best two results on the right for each evaluation protocol by using the equal error rate (EER) threshold to calculate the accuracy of each experiment. The visualization marks the misclassified bona-fide and PAI samples based on the EER threshold and shows the corresponding locations of these samples in the mean-intensity feature visualization. Finally, the codes of the misclassified PAIs are presented in the legends. This analysis results in the following observations:

- The addition of sensing modalities leads to performance improvement, in most cases (compare rightmost to leftmost input channels), consistent with the ROC curve observations.
- The mean-intensity feature visualization indeed provides an estimate of how challenging a dataset is. The majority of misclassified PAIs by the FCN model are in most cases within the bona-fide cluster of the mean-intensity t-SNE visualization. This dictates that intensities of multi-spectral data could be playing an important role as classification features in the model.
- The majority of misclassified bona-fides lie at the border of the bona-fide cluster in the mean-intensity feature visualization, which further supports the aforementioned argument (this is mostly visible in the inter-site experiment).
- The misclassified PAI codes for the rightmost highest accuracy experiments agree with the analysis of Fig. 7, which demonstrated that the most challenging PAIs are the transparent overlays (see Table 2).
- The left-most experiments also demonstrate the ability of deep features to achieve a reasonable classification performance even when large amounts of intensity features are intermingled for the two classes.
- Finally, the inter-site analysis clearly shows a shift in the EER threshold resulting from the vastly different demographics and collection system variations for the two datasets. This is consistent with the mean-

intensity t-SNE separation of bona-fide samples from different datasets in Fig. 7.

6 CONCLUSIONS

This paper presented a comprehensive analysis of *hybrid (hardware-based)* FPAD, using a number of recently introduced sensing modalities, which are front-illuminated visible, NIR, and SWIR images; back-illuminated NIR images, and laser-speckle contrast imaging. The analysis was conducted on a new dataset, named *PADISI-Finger*. *PADISI-Finger* consists of two collections performed at two different sites, *PADISI-USC* and *PADISI-APL*, the former of which will be publicly released upon the acceptance of this manuscript. *PADISI-Finger* contains data from over a thousand participants and covers more than 60 PAI species. Our analysis employed a novel fully-convolutional network model, whose power was demonstrated by showing its state-of-the-art performance on the LivDet2015 dataset. FPAD performance using this FCN model revealed the advantages of some of the individual unconventional sensing modalities and all different combinations of them over legacy data. The power of combining multiple sensing modalities was further confirmed by the results of our rigorous evaluation protocols, which assessed the effects of testing on completely unseen attack categories (leave-one-attack out) as well as under different dataset characteristics (inter-collection). In such challenging protocols, front-illuminated multi-spectral images (visible, NIR, and SWIR) stood out as the most reliable sensing modalities, either individually or in combination with others. Low-dimensional data visualization of the raw average intensity values revealed a notable similarity to the equivalent visualization of the features learned by the FCN model, which upholds the role of the data in the obtained FPAD performance in our analysis. Finally, it was observed that the FPAD performance is not directly correlated with the number of employed sensing modalities. This is believed to be an artifact of the neural network model architecture, and its investigation is deferred to our future work.

ACKNOWLEDGMENTS

This research is based upon work supported by the Office of the Director of National Intelligence (ODNI), Intelligence Advanced Research Projects Activity (IARPA), via IARPA R&D Contract No. 2017-17020200005. The views and conclusions contained herein are those of the authors and should not be interpreted as necessarily representing the official policies or endorsements, either expressed or implied, of the ODNI, IARPA, or the U.S. Government. The U.S. Government is authorized to reproduce and distribute reprints for Governmental purposes notwithstanding any copyright annotation thereon.

The authors would also like to acknowledge the efforts of the APL team for organizing and managing the large scale data collection at their site in Columbia, Maryland, and the effort of our collaborators from Hochschule Darmstadt University of Applied Sciences for their help and support in collecting fingerprint data at the APL site. A final acknowledgement is due to Mian Zhong and Hanchen Xie for their efforts towards a very early draft of this manuscript.

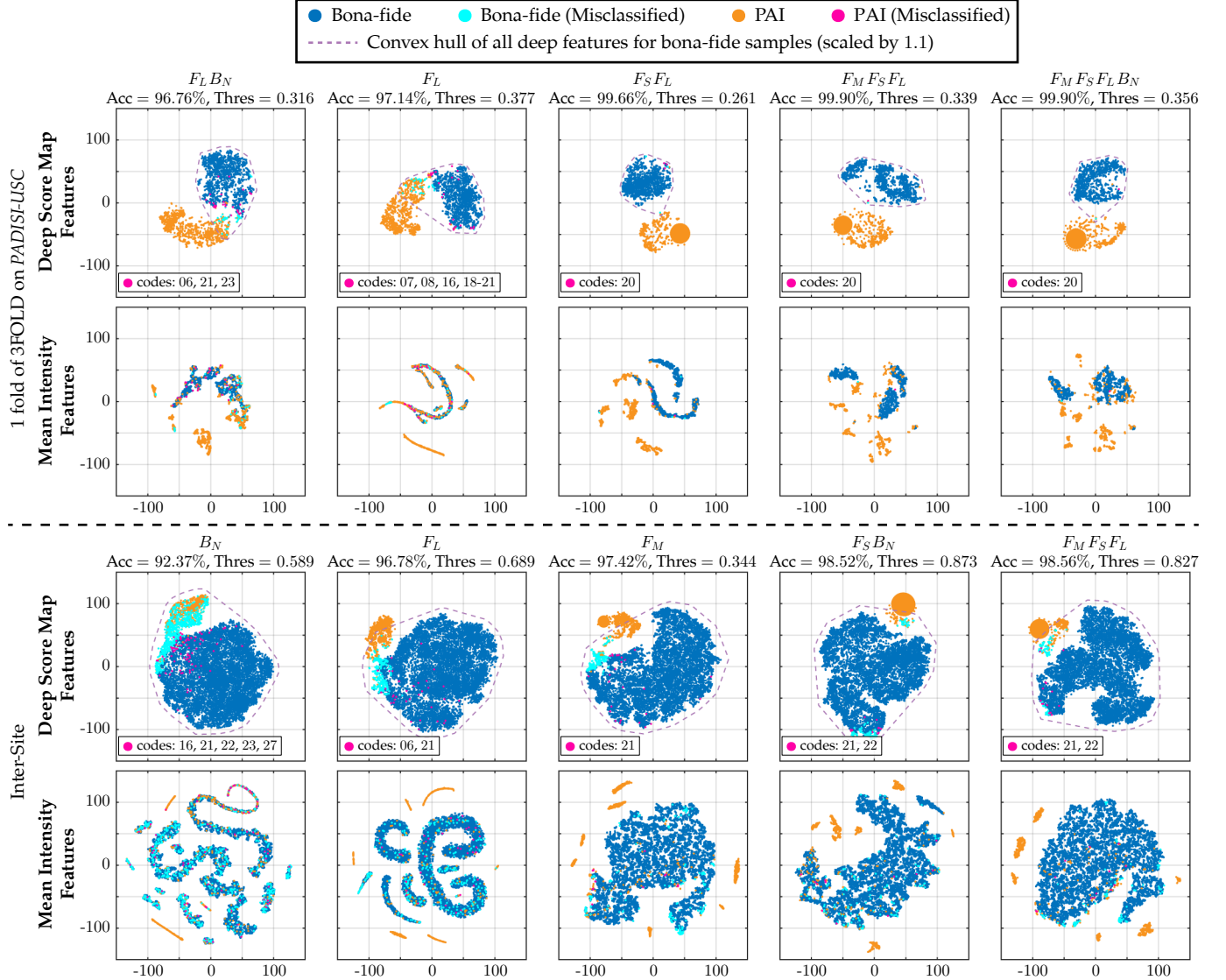


Fig. 14. t-SNE visualization comparison for deep features (score maps) of the FCN model in Fig. 8 and the corresponding mean-intensity features of the utilized input channels. Each experiment presents the classification accuracy based on the EER threshold, the misclassified samples of the FCN model in both visualizations and the codes of misclassified PAIs in the legend. Experiments are sorted by their accuracy from left to right. The reader is referred to Section 5.2.3 for a detailed analysis.

REFERENCES

- [1] S. Marcel, M. S. Nixon, J. Fierrez, and N. W. D. Evans, Eds., *Handbook of Biometric Anti-Spoofing - Presentation Attack Detection, Second Edition*, ser. Advances in Computer Vision and Pattern Recognition. Springer, 2019. [Online]. Available: <https://doi.org/10.1007/978-3-319-92627-8>
- [2] A. K. Jain, K. Nandakumar, and A. Ross, "50 years of biometric research: Accomplishments, challenges, and opportunities," *Pattern Recognition Letters*, vol. 79, pp. 80 – 105, 2016. [Online]. Available: <http://www.sciencedirect.com/science/article/pii/S0167865515004365>
- [3] A. Ross and A. Jain, "Human recognition using biometrics: An overview," *Annales des Telecommunications*, vol. 62, no. 1-2, pp. 11–35, 1 2007.
- [4] J. Galbally, J. Fierrez, , and J. Ortega-Garcia, "Vulnerabilities in biometric systems: attacks and recent advances in liveness detection," in *Spanish Workshop on Biometrics, SWB*, 2007.
- [5] E. Bowden-Peters, R. C. W. Phan, J. N. Whitley, and D. J. Parish, *Fooling a Liveness-Detecting Capacitive Fingerprint Scanner*. Springer Berlin Heidelberg, 2012, pp. 484–490. [Online]. Available: https://doi.org/10.1007/978-3-642-28368-0_32
- [6] E. Marasco and A. Ross, "A survey on antispoofing schemes for fingerprint recognition systems," *ACM Comput. Surv.*, vol. 47, no. 2, pp. 28:1–28:36, Nov. 2014. [Online]. Available: <http://doi.acm.org/10.1145/2617756>
- [7] C. Sousedik and C. Busch, "Presentation attack detection methods for fingerprint recognition systems: a survey," *IET Biometrics*, vol. 3, no. 4, pp. 219–233, 2014. [Online]. Available: <https://doi.org/10.1049/iet-bmt.2013.0020>
- [8] S. Nikam and S. Agarwal, "Fingerprint liveness detection using curvelet energy and co-occurrence signatures," in *2008 Fifth International Conference on Computer Graphics, Imaging and Visualisation*, Aug 2008, pp. 217–222.
- [9] C. Zaghetto, M. Mendelson, A. Zaghetto, and F. d. B. Vidal, "Liveness detection on touchless fingerprint devices using texture descriptors and artificial neural networks," in *2017 IEEE International Joint Conference on Biometrics (IJCB)*, Oct 2017, pp. 406–412.
- [10] B. Tan and S. Schuckers, "Spoofing protection for fingerprint scanner by fusing ridge signal and valley noise," *Pattern Recognition*, vol. 43, no. 8, pp. 2845 – 2857, 2010. [Online]. Available: <http://www.sciencedirect.com/science/article/pii/S0031320310000993>
- [11] S. Memon, N. Manivannan, and W. Balachandran, "Active pore detection for liveness in fingerprint identification system," in *2011*

- 19th Telecommunications Forum (TELFOR) Proceedings of Papers, Nov 2011, pp. 619–622.
- [12] J. Galbally, F. Alonso-Fernandez, J. Fierrez, and J. Ortega-Garcia, “A high performance fingerprint liveness detection method based on quality related features,” *Future Generation Computer Systems*, vol. 28, no. 1, pp. 311 – 321, 2012. [Online]. Available: <http://www.sciencedirect.com/science/article/pii/S0167739X1000244X>
- [13] A. Antonelli, R. Cappelli, D. Maio, and D. Maltoni, “Fake finger detection by skin distortion analysis,” *IEEE Transactions on Information Forensics and Security*, vol. 1, no. 3, pp. 360–373, Sept 2006.
- [14] A. Abhyankar and S. Schuckers, “Integrating a wavelet based perspiration liveness check with fingerprint recognition,” *Pattern Recogn.*, vol. 42, no. 3, pp. 452–464, Mar. 2009. [Online]. Available: <http://dx.doi.org/10.1016/j.patcog.2008.06.012>
- [15] P. V. Reddy, A. Kumar, S. M. K. Rahman, and T. S. Mundra, “A new method for fingerprint antispoofing using pulse oximetry,” in *2007 First IEEE International Conference on Biometrics: Theory, Applications, and Systems*, Sept 2007, pp. 1–6.
- [16] D. Baldisserra, A. Franco, D. Maio, and D. Maltoni, “Fake fingerprint detection by odor analysis,” in *International Conference on Advances in Biometrics*. Berlin, Heidelberg: Springer-Verlag, 2006, pp. 265–272. [Online]. Available: http://dx.doi.org/10.1007/11608288_36
- [17] Y. Cheng and K. V. Larin, “Artificial fingerprint recognition by using optical coherence tomography with autocorrelation analysis,” *Appl. Opt.*, vol. 45, no. 36, pp. 9238–9245, Dec 2006. [Online]. Available: <http://ao.osa.org/abstract.cfm?URI=ao-45-36-9238>
- [18] T. van der Putte and J. Keuning, *Biometrical Fingerprint Recognition: Don't get your Fingers Burned*. Boston, MA: Springer US, 2000, pp. 289–303. [Online]. Available: https://doi.org/10.1007/978-0-387-35528-3_17
- [19] T. Matsumoto, H. Matsumoto, K. Yamada, and S. Hoshino, “Impact of artificial “gummy” fingers on fingerprint systems,” in *Proc. SPIE*, vol. 4677, 2002, pp. 4677 – 4677 – 15. [Online]. Available: <https://doi.org/10.1117/12.462719>
- [20] C. Barral and A. Tria, *Fake Fingers in Fingerprint Recognition: Glycerin Supersedes Gelatin*. Berlin, Heidelberg: Springer Berlin Heidelberg, 2009, pp. 57–69. [Online]. Available: https://doi.org/10.1007/978-3-642-02002-5_4
- [21] C. Barral, “Biometrics & security: Combining fingerprints, smart cards and cryptography,” Ph.D. dissertation, EPFL, Lausanne, Switzerland, 2010.
- [22] A. Roy, N. Memon, J. Togelius, and A. Ross, “Evolutionary methods for generating synthetic MasterPrint templates: Dictionary attack in fingerprint recognition,” in *2018 International Conference on Biometrics (ICB)*, February 2018.
- [23] P. Bontrager, , A. Roy, J. Togelius, N. Memon, and A. Ross, “Deep-MasterPrints: Generating masterprints for dictionary attacks via latent variable evolution,” in *IEEE 9th International Conference on Biometrics: Theory, Applications and Systems (BTAS)*, October 2018.
- [24] P. Johnson and S. Schuckers, “Evaluation of presentation attack detection: An example,” in *Proceedings of the International Biometric Performance Conference*, ser. IBPC, 2014.
- [25] N. K. Ratha, J. H. Connell, and R. M. Bolle, “Enhancing security and privacy in biometrics-based authentication systems,” *IBM Systems Journal*, vol. 40, no. 3, pp. 614–634, 2001.
- [26] L. Spinoulas, M. Hussein, D. Geissbühler, J. Mathai, O. G. Almeida, G. Clivaz, S. Marcel, and W. AbdAlmageed, “Multispectral Biometrics System Framework: Application to Presentation Attack Detection,” *CoRR*, 2020.
- [27] M. E. Hussein, L. Spinoulas, F. Xiong, and W. Abd-Almageed, “Fingerprint presentation attack detection using a novel multispectral capture device and patch-based convolutional neural networks,” in *2018 IEEE International Workshop on Information Forensics and Security (WIFS)*, Dec 2018, pp. 1–8.
- [28] H. Mirzaalian, M. Hussein, and W. Abd-Almageed, “On the effectiveness of laser speckle contrast imaging and deep neural networks for detecting known and unknown fingerprint presentation attacks,” in *2019 International Conference on Biometrics (ICB)*, June 2019, pp. 1–8.
- [29] V. Mura, L. Ghiani, G. L. Marcialis, and F. Roli, “LivDet 2015 fingerprint liveness detection competition 2015,” *BTAS*, 2015.
- [30] S. S. Kulkarni and H. Y. Patil, “Survey on fingerprint spoofing, detection techniques and databases,” *International Journal of Computer Applications*, vol. 95, no. C, pp. 30–33, 2017.
- [31] M. Drahansky, “Experiments with skin resistance and temperature for liveness detection,” in *2008 International Conference on Intelligent Information Hiding and Multimedia Signal Processing*, 2008, pp. 1075–1079.
- [32] E. Marasco and C. Sansone, “Combining perspiration- and morphology-based static features for fingerprint liveness detection,” *Pattern Recogn. Lett.*, vol. 33, no. 9, pp. 1148–1156, Jul. 2012. [Online]. Available: <http://dx.doi.org/10.1016/j.patrec.2012.01.009>
- [33] J. N. Hogan, “Optical coherence tomography array based subdermal imaging device,” US Patent App. 16/225,278, 2019.
- [34] T. Chugh and A. K. Jain, “OCT fingerprints: Resilience to presentation attacks,” *ArXiv*, vol. abs/1908.00102, 2019.
- [35] A. Shiratsuki, E. Sano, M. Shikai, T. Nakashima, T. Takashima, M. Ohmi, and M. Haruna, “Novel optical fingerprint sensor utilizing optical characteristics of skin tissue under fingerprints,” *Biomedical Optics*, p. 8087, 2005.
- [36] R. Tolosana, M. Gomez-Barrero, J. Kolberg, A. Morales, C. Busch, and J. Ortega-Garcia, “Towards fingerprint presentation attack detection based on convolutional neural networks and short wave infrared imaging,” in *2018 International Conference of the Biometrics Special Interest Group (BIOSIG)*, Sep. 2018, pp. 1–5.
- [37] R. K. Rowe and D. P. Sidlauskas, “Multispectral biometric sensor,” US Patent 7,147,153, 2006.
- [38] R. K. Rowe, K. A. Nixon, and P. W. Butler, *Multispectral Fingerprint Image Acquisition*. Springer London, 2008, pp. 3–23. [Online]. Available: https://doi.org/10.1007/978-1-84628-921-7_1
- [39] D. Maltoni, D. Maio, A. K. Jain, and S. Prabhakar, *Handbook of Fingerprint Recognition*, 2nd ed. Springer Publishing Company Incorporated, 2009.
- [40] C. Hengfoss, A. Kulcke, G. Mull, C. Edler, K. Pschel, and E. Jopp, “Dynamic liveness and forgeries detection of the finger surface on the basis of spectroscopy in the 400–1650nm region,” *Forensic Science International*, vol. 212, no. 1, pp. 61 – 68, 2011. [Online]. Available: <http://www.sciencedirect.com/science/article/pii/S0379073811002295>
- [41] M. Drahansky, M. Dolezel, J. Vana, E. Brezinova, J. Yim, and K. Shim, “New optical methods for liveness detection on fingers,” *BioMed research international*, vol. 2013, p. 197925, 09 2013.
- [42] R. Tolosana, M. Gomez-Barrero, C. Busch, and J. Ortega-Garcia, “Biometric presentation attack detection: Beyond the visible spectrum,” *IEEE Transactions on Information Forensics and Security*, vol. 15, pp. 1261–1275, 2020.
- [43] J. J. Engelsma, K. Cao, and A. K. Jain, “Raspireader: Open source fingerprint reader,” *IEEE Transactions on Pattern Analysis and Machine Intelligence*, vol. 41, no. 10, pp. 2511–2524, Oct 2019.
- [44] J. Jia, L. Cai, K. Zhang, and D. Chen, “A new approach to fake finger detection based on skin elasticity analysis,” in *International Conference on Advances in Biometrics*. Berlin, Heidelberg: Springer-Verlag, 2007, pp. 309–318. [Online]. Available: <http://dl.acm.org/citation.cfm?id=2391659.2391694>
- [45] P. Lapsley, J. Less, D. Pare, and N. Hoffman, “Anti-fraud biometric sensor that accurately detects blood flow,” US Patent: 5737439, 1998.
- [46] P. G. Vaz, A. Humeau-Heurtier, E. Figueiras, C. Correia, and J. Cardoso, “Laser speckle imaging to monitor microvascular blood flow: A review,” *IEEE Reviews in Biomedical Engineering*, vol. 9, pp. 106–120, 2016.
- [47] S. B. Nikam and S. Agarwal, “Local binary pattern and wavelet-based spoof fingerprint detection,” *Int. J. Biometrics*, vol. 1, pp. 141–159, 2008.
- [48] R. Derakhshani, S. Schuckers, L. Hornak, and L. O. Gorman, “Neural network-based approach for detection of liveness in fingerprint scanners,” *Pattern Recognition*, vol. 36, no. 2, pp. 383–396, 2003.
- [49] B. Tan and S. Schuckers, “Liveness detection for fingerprint scanners based on the statistics of wavelet signal processing,” in *Computer Vision and Pattern Recognition Workshop*, June 2006, pp. 26–26.
- [50] P. Keilbach, J. Kolberg, M. Gomez-Barrero, C. Busch, and H. Langweg, “Fingerprint presentation attack detection using laser speckle contrast imaging,” in *2018 International Conference of the Biometrics Special Interest Group (BIOSIG)*, Sep. 2018, pp. 1–6.
- [51] L. Ghiani, A. Hadid, G. L. Marcialis, and F. Roli, “Fingerprint liveness detection using binarized statistical image features,” in *2013 IEEE Sixth International Conference on Biometrics: Theory, Applications and Systems (BTAS)*, Sep. 2013, pp. 1–6.

- [52] L. J. González-Soler, M. Gomez-Barrero, L. Chang, A. P. Surez, and C. Busch, "On the impact of different fabrication materials on fingerprint presentation attack detection," in *2019 International Conference on Biometrics (ICB)*, 2019, pp. 1–6.
- [53] M. Gomez-Barrero, J. Kolberg, and C. Busch, "Multi-Modal Fingerprint Presentation Attack Detection: Analysing the Surface and the Inside," in *2019 International Conference on Biometrics (ICB)*, June 2019, pp. 1–8.
- [54] D. Gragnaniello, G. Poggi, C. Sansone, and L. Verdoliva, "Fingerprint liveness detection based on weber local image descriptor," in *2013 IEEE Workshop on Biometric Measurements and Systems for Security and Medical Applications*, Sep. 2013, pp. 46–50.
- [55] D. Gragnaniello, G. Poggi, C. Sansone, and L. Verdoliva, "Local contrast phase descriptor for fingerprint liveness detection," *Pattern Recogn.*, vol. 48, no. 4, pp. 1050–1058, Apr. 2015. [Online]. Available: <http://dx.doi.org/10.1016/j.patcog.2014.05.021>
- [56] G. L. Marcialis, F. Roli, and A. Tidu, "Analysis of fingerprint pores for vitality detection," in *2010 20th International Conference on Pattern Recognition*, Aug 2010, pp. 1289–1292.
- [57] F. Pala and B. Bhanu, *Deep Triplet Embedding Representations for Liveness Detection*. Cham: Springer International Publishing, 2017, pp. 287–307. [Online]. Available: https://doi.org/10.1007/978-3-319-61657-5_12
- [58] R. Nogueira, R. de Alencar Lotufo, and R. Machado, "Fingerprint liveness detection using convolutional neural networks," *IEEE Trans. Inf. Forensics Secur.*, vol. 11, no. 6, pp. 1206–1213, 2016.
- [59] R. Gajjawada, A. Popli, T. Chugh, A. Namboodiri, and A. K. Jain, "Universal material translator: Towards spoof fingerprint generalization," in *2019 International Conference on Biometrics (ICB)*, 2019, pp. 1–8.
- [60] D. Menotti, G. Chiachia, A. S. Pinto, W. R. Schwartz, H. Pedrini, A. X. Falca, and A. Rocha, "Deep representations for iris, face, and fingerprint spoofing detection," *Information Forensics and Security*, vol. 10, p. 864879, 2015.
- [61] A. Krizhevsky, I. Sutskever, and G. E. Hinton, "ImageNet Classification with Deep Convolutional Neural Networks," in *Advances in Neural Information Processing Systems 25*, F. Pereira, C. J. C. Burges, L. Bottou, and K. Q. Weinberger, Eds. Curran Associates, Inc., 2012, pp. 1097–1105.
- [62] K. Simonyan and A. Zisserman, "Very deep convolutional networks for large-scale image recognition," *CoRR*, vol. 1409, 2014.
- [63] C. Wang, K. Li, Z. Wu, and Q. Zhao, "A DCNN based fingerprint liveness detection algorithm with voting strategy," *Chinese Conference on Biometric Recognition*, vol. 35, pp. 241–249, 2015.
- [64] B. Bhanu and A. Kumar, *Deep Learning for Biometrics*, 1st ed. Springer Publishing Company, Incorporated, 2017.
- [65] T. Chugh, K. Cao, and A. K. Jain, "Fingerprint Spoof Buster: Use of minutiae-centered patches," *IEEE Transactions on Information Forensics and Security*, vol. 13, no. 9, pp. 2190–2202, 2018.
- [66] T. Chugh and A. K. Jain, "Fingerprint presentation attack detection: Generalization and efficiency," in *2019 International Conference on Biometrics (ICB)*, 2019, pp. 1–8.
- [67] T. Chugh, K. Cao, and A. K. Jain, "Fingerprint spoof detection using minutiae-based local patches," in *2017 IEEE International Joint Conference on Biometrics (IJCB)*, 2017, pp. 581–589.
- [68] E. Park, X. Cui, W. Kim, and H. Kim, "End-to-end fingerprints liveness detection using convolutional networks with gram module," *CoRR*, vol. abs/1803.07830, 2018. [Online]. Available: <http://arxiv.org/abs/1803.07830>
- [69] S. Kim, B. Park, B. S. Song, and S. Yang, "Deep belief network based statistical feature learning for fingerprint liveness detection," *Pattern Recognition Letters*, vol. 77, pp. 58 – 65, 2016. [Online]. Available: <http://www.sciencedirect.com/science/article/pii/S0167865516300198>
- [70] J. Kolberg, M. Gomez-Barrero, and C. Busch, "Multi-algorithm benchmark for fingerprint presentation attack detection with laser speckle contrast imaging," in *2019 International Conference of the Biometrics Special Interest Group (BIOSIG)*, 2019, pp. 1–5.
- [71] Y. Mao, S. Chang, K. Larin, Q. Xiao, W. Almuhtadi, and C. Flueraru, "Fingerprint spoof detection by NIR optical analysis," in *State of the art in Biometrics*, L. Nanni, Ed. Rijeka: InTech, 2011, ch. 3. [Online]. Available: <https://doi.org/10.5772/19453>
- [72] "Basler acA1300-60gmNIR," <https://www.baslerweb.com/en/products/cameras/area-scan-cameras/ace/aca1300-60gmnir/>.
- [73] "Xenics Bobcat 320 GigE 100," <https://www.xenics.com/products/bobcat-320-series/>.
- [74] "Eblana Photonics, EP1310-ADF-DX1-C-FM," <https://www.eblanaphotonics.com/fiber-comms.php>.
- [75] D. W. A. Catherine C. Cooksey, Benjamin K. Tsai, "A collection and statistical analysis of skin reflectance signatures for inherent variability over the 250 nm to 2500 nm spectral range," in *SPIE Defense, Security & Sensing*, vol. 9082, May 2014, pp. 9082 – 11. [Online]. Available: <https://doi.org/10.1117/12.2053604>
- [76] H. Steiner, A. Kolb, and N. Jung, "Reliable face anti-spoofing using multispectral SWIR imaging," in *2016 International Conference on Biometrics (ICB)*, 2016, pp. 1–8.
- [77] M. Gomez-Barrero, J. Kolberg, and C. Busch, "Towards fingerprint presentation attack detection based on short wave infrared imaging and spectral signatures," in *Proceedings of the 11th Norwegian Information Security Conference*, 2018.
- [78] M. Gomez-Barrero and C. Busch, "Multi-spectral convolutional neural networks for biometric presentation attack detection," in *Proceedings of the 12th Norwegian Information Security Conference*, 2019.
- [79] D. Briers, D. D. Duncan, E. Hirst, S. Kirkpatrick, M. Larsson, W. Steenbergen, T. Stromberg, and O. Thompson, "Laser speckle contrast imaging: Theoretical and practical limitations," *Journal of biomedical optics*, vol. 18, p. 66018, 06 2013.
- [80] A. Chatterjee, V. Bhatia, and S. Prakash, "Anti-spoof touchless 3D fingerprint recognition system using single shot fringe projection and biospeckle analysis," *Optics and Lasers in Engineering*, vol. 95, no. C, pp. 1–7, 2017.
- [81] A. M. Badawi, "Hand vein biometric verification prototype: A testing performance and patterns similarity," in *IPCV*, 2006.
- [82] J. Kolberg, M. Gomez-Barrero, S. Venkatesh, R. Ramachandra, and C. Busch, *Presentation Attack Detection for Finger Recognition*. Cham: Springer International Publishing, 2020, pp. 435–463. [Online]. Available: https://doi.org/10.1007/978-3-030-27731-4_14
- [83] M. Gomez-Barrero, J. Kolberg, and C. Busch, "Towards multi-modal finger presentation attack detection," in *2018 14th International Conference on Signal-Image Technology Internet-Based Systems (SITIS)*, 2018, pp. 547–552.
- [84] L. van der Maaten and G. Hinton, "Visualizing high-dimensional data using t-SNE," *Journal of Machine Learning Research*, vol. 9, no. nov, pp. 2579–2605, 2008.
- [85] D. P. Kingma and J. Ba, "Adam: A Method for Stochastic Optimization," in *3rd International Conference on Learning Representations, ICLR 2015, San Diego, CA, USA, May 7-9, 2015, Conference Track Proceedings*, Y. Bengio and Y. LeCun, Eds., 2015. [Online]. Available: <http://arxiv.org/abs/1412.6980>
- [86] <https://www.iarpa.gov/index.php/research-programs/odin>.
- [87] *Information technology – Biometric presentation attack detection – Part 3: Testing and reporting*, International Organization for Standardization, 2017.
- [88] A. G. Roy, N. Navab, and C. Wachinger, "Concurrent spatial and channel 'Squeeze & Excitation' in fully convolutional networks," in *Medical Image Computing and Computer Assisted Intervention – MICCAI 2018*, A. F. Frangi, J. A. Schnabel, C. Davatzikos, C. Alberola-López, and G. Fichtinger, Eds. Cham: Springer International Publishing, 2018, pp. 421–429.
- [89] S. Woo, J. Park, J.-Y. Lee, and I. S. Kweon, "CBAM: Convolutional block attention module," in *Computer Vision – ECCV 2018*, V. Ferrari, M. Hebert, C. Sminchisescu, and Y. Weiss, Eds. Cham: Springer International Publishing, 2018, pp. 3–19.
- [90] Y. Zhang, M. Fang, and N. Wang, "Channel-spatial attention network for fewshot classification," *PLOS ONE*, vol. 14, no. 12, pp. 1–16, 12 2019. [Online]. Available: <https://doi.org/10.1371/journal.pone.0225426>



Leonidas Spinoulas Leonidas Spinoulas received his Diploma degree in Electrical and Computer Engineering from the National Technical University of Athens, Greece in 2010. In September 2010 he joined Northwestern University, Evanston, IL, USA and the Image and Video Processing Laboratory (IVPL) under the supervision of Prof. Aggelos K. Katsaggelos. He received the M. Sc. Degree in Electrical Engineering and Computer Science in 2012 and the Ph.D. degree from the same department in August 2016. Since 2017, he holds a Research Computer Scientist position with the Information Sciences Institute (University of Southern California), Marina del Rey, CA. He was previously a Research Scientist for Ricoh Innovations Corporation, Cupertino, CA, USA. He was the recipient of the best paper awards at EUSIPCO 2013 and SENSORCOMM 2015 and has 4 patents. His primary research interests include deep learning, biometrics, multispectral imaging, image processing, image restoration, inverse problems and compressive sensing.



Wael AbdAlmageed Dr. AbdAlmageed is a Research Associate Professor at the Department of Electrical and Computer Engineering, and a research Team Leader and Supervising Computer Scientist with Information Sciences Institute, both being units of USC Viterbi School of Engineering. His research interests include representation learning, debiasing and fair representations, multimedia forensics and visual misinformation (including deepfake and image manipulation detection) and biometrics. Prior to joining ISI, Dr. AbdAlmageed was a research scientist with the University of Maryland at College Park, where he led several research efforts for various NSF, DARPA and IARPA programs. He obtained his Ph.D. with Distinction from the University of New Mexico in 2003 where he was also awarded the Outstanding Graduate Student award. He has two patents and over 70 publications in top computer vision and high performance computing conferences and journals. Dr. AbdAlmageed is the recipient of 2019 USC Information Sciences Institute Achievement Award.



Hengameh Mirzaalian Hengameh Mirzaalian conducts research on image-processing, machine-learning, and deep-learning techniques to address different tasks on images with different modalities and applications. She received her Ph.D. in computing science from Simon Fraser University, BC. Prior to ISI, she worked with various research institutes including Siemens Corporate Research and Technologies, Harvard Medical School, Boston Childrens Hospital, Brigham and Womens

Hospital and Nasa Jet Propulsion Laboratory. Her research appeared on top journals including Medical Image Analysis, NeuroImage and IEEE conferences.



Mohamed Hussein Dr. Mohamed E. Hussein is a computer scientist at USC ISI and an associate professor (on leave) at Alexandria University, Egypt. Dr. Hussein obtained his Ph.D. degree in Computer Science from the University of Maryland at College Park, MD, USA in 2009. Then, he spent close to two years as an Adjunct Member Research Staff at Mitsubishi Electric Research Labs, Cambridge, MA, before moving to Alexandria University as a faculty member. Prior to joining ISI, he spent three years at Egypt-Japan

University of Science and Technology (E-JUST), in Alexandria, Egypt. Dr. Hussein's most recent research focus has been in securing biometrics and machine learning systems. He has over 30 published papers, and three issued patents.